Electromagnetic extension of the Dory-Guest-Harris instability as a benchmark for Vlasov-Maxwell continuum kinetic simulations of magnetized plasmas^{a)}

I. A. M. Datta, 1, b) D. W. Crews, 1, c) and U. Shumlak 1, d)

Computational Plasma Dynamics Laboratory, Aerospace and Energetics Research Program, University of Washington, Seattle, WA 98195, United States

(Dated: 5 August 2021)

A closed-form integral representation of the electromagnetic dispersion relation for plasma waves propagating perpendicular to a magnetic field is derived. Growth rates and oscillation frequencies are calculated for several cases of the Dory-Guest-Harris instability and compared with those calculated from the usual electrostatic version of the dispersion relation. The comparisons show that the electromagnetic treatment more accurately identifies unstable configurations in plasmas with high beta, where the electrostatic dispersion relation predicts stability. Continuum kinetic simulations using the WARPXM framework confirm the theoretical calculations. The electromagnetic extension of the Dory-Guest-Harris instability provides a new benchmark problem for testing continuum kinetic simulations using the Vlasov-Maxwell plasma model, including for other numerical treatments such as particle-in-cell methods.

a) Published as Physics of Plasmas 28 (7), 072112 (2021). doi.org/10.1063/5.0057230

b)idatta@uw.edu

c)dcrews@uw.edu

d)shumlak@uw.edu

I. INTRODUCTION

The development and application of continuum kinetic codes to solve Vlasov-Poisson and Vlasov-Maxwell systems has increased in recent years, 1-3 as has the need for standardized benchmark problems to evaluate code accuracy. Most existing benchmark problems are based on the electrostatic assumption and are suitable for Vlasov-Poisson solvers. However, there is a dearth of benchmark problems for the more general electromagnetic theory used for Vlasov-Maxwell solvers. One such candidate problem is the Dory-Guest-Harris (DGH) instability, which is a phenomenon closely related to Bernstein modes.⁴ The DGH instability is known to arise from electrostatic waves propagating perpendicular to a magnetic field for certain probability distribution functions of a plasma, causing strong resonances at ion and electron cyclotron frequencies.^{5,6} The probability distribution functions are often of loss cone or ring-type in velocity space and are found in various situations ranging from magnetic mirror confinement devices^{7,8} to Earth's magnetosphere.^{9–11} The excitation of waves at harmonics of the cyclotron frequency arising from the DGH instability can also be used to heat plasmas in magnetic confinement devices such as tokamaks¹² as well as for diagnostics to measure electron temperatures in these types of devices¹³ or the magnetic field strength in the ionosphere. 14

Previous work used the DGH instability as a benchmark for a 1D2V continuum Vlasov-Poisson finite volume method by deriving a closed-form integral representation of the dispersion relation for perpendicular electrostatic waves and then comparing numerical solutions to quantify agreement and convergence. This study is expanded to include electromagnetic effects by analyzing the DGH instability in the context of a Vlasov-Maxwell plasma model. The results show where the instability deviates from electrostatic behavior and produces electromagnetic effects associated with perturbations to the magnetic field. The rest of this paper is outlined as follows. Section II gives an overview of the Vlasov-Maxwell model for kinetic plasmas. Section III derives the electromagnetic dispersion relation associated with perpendicular waves for probability distribution functions of the form $f(v_{\perp})$. The electromagnetic and electrostatic dispersion relations are compared for several illustrative cases in Sec. IV. Section V summarizes a numerical method used to solve the full Vlasov-Maxwell system using a continuum Eulerian discontinuous Galerkin method. Section VI highlights results from simulations and comparisons with the electromagnetic and electrostatic dispersions with the electromagnetic and electrostatic dispersions.

sion relations. Conclusions are given in Sec. VII.

II. GOVERNING EQUATIONS OF THE VLASOV-MAXWELL SYSTEM

The Vlasov-Maxwell system is described by the Vlasov equation

$$\frac{\partial f_s}{\partial t} + \boldsymbol{v} \cdot \nabla f_s + (\omega_c \tau) \frac{Z_s}{A_s} (\boldsymbol{E} + \boldsymbol{v} \times \boldsymbol{B}) \cdot \nabla_{\boldsymbol{v}} f_s = 0, \tag{1}$$

written for each species s in phase space, and Maxwell's equations in physical space, given by Ampere's law

$$\frac{\partial \mathbf{E}}{\partial t} - \frac{(\omega_p \tau)^2}{(\omega_c \tau)^2} \nabla \times \mathbf{B} = -\frac{(\omega_p \tau)^2}{(\omega_c \tau)} \mathbf{j} = -\frac{(\omega_p \tau)^2}{(\omega_c \tau)} \sum_s Z_s \int \mathbf{v} f_s(\mathbf{x}, \mathbf{v}, t) d\mathbf{v}, \tag{2}$$

and Faraday's law

$$\frac{\partial \mathbf{B}}{\partial t} + \nabla \times \mathbf{E} = 0. \tag{3}$$

These equations are written in a normalized form, involving a non-dimensional mass $A_s = \frac{m_s}{m_0}$ and non-dimensional charge $Z_s = \frac{q_s}{q_0}$. Normalized reference plasma frequency $\omega_p \tau = \sqrt{\frac{q_0^2 n_0}{m_0 \epsilon_0}} \tau$ and cyclotron frequency $\omega_c \tau = \frac{q_0 B_0}{m_0} \tau$ are introduced, where τ is a reference timescale. The reference velocity is tied to the thermal speed, which also specifies a reference length scale such that $v_0 = \frac{L}{\tau} = \sqrt{\frac{T_0}{m_0}}$, where T_0 is expressed in units of energy. The relation $\frac{B_0^2}{\mu_0} = n_0 T_0$ connects B_0 to n_0 and T_0 . This normalization is advantageous for this problem as neither the plasma oscillation nor the cyclotron frequency is inherently favored over the other in this formulation. Further details on this normalization can be found in Ref. [15]. Since the electron dynamics are the focus of the DGH instability, the normalizing mass is that of the electrons, $m_0 = m_e$, and the normalizing charge is the elementary charge, $q_0 = e$. In cases where the ion dynamics are of interest, the analysis can be repeated using ions as the normalizing species.

III. LINEAR ANALYSIS OF ELECTROMAGNETIC $k_{\parallel}=0$ WAVES IN UNIFORMLY MAGNETIZED PLASMA

The electromagnetic dispersion relation for the DGH instability is derived by perturbing the Vlasov-Maxwell system about a spatially uniform equilibrium plasma state, $f_s^0(\mathbf{v})$, and

a uniform magnetic field, \mathbf{B}^0 , which leads to equilibrium cyclotron motion. The response of this equilibrium can be analyzed using the linearized form of the governing Eqs. (1), (2), and (3). In the linearization procedure, the fields and probability distribution function are expressed as a sum of the equilibrium and perturbation components: $\mathbf{E} = \mathbf{E}^0 + \mathbf{E}^1$, $\mathbf{B} = \mathbf{B}^0 + \mathbf{B}^1$, $f_s = f_s^0 + f_s^1$, where the perturbed quantities are assumed to be much smaller in magnitude than the equilibrium quantities such that nonlinear products of perturbations can be neglected. For the electric field, it is sufficient to assume there is no equilibrium component ($\mathbf{E} = \mathbf{E}^1$). Except for strong equilibrium electric fields ($\mathbf{E}^0 \geq \frac{c}{v_0} \mathbf{B}^0$), it is always possible to set \mathbf{E}^0 to any arbitrary value by transforming to a different frame of reference using the relationship $\mathbf{E}^0 + \mathbf{v} \times \mathbf{B}^0 = 0$, where \mathbf{v} is the parameter for the Galilean transform of the distribution function. With the probability distribution function and fields being expressed through the summation of the equilibrium and perturbation components, the first-order linearized expansions of Eqs. (1), (2), and (3) are

$$\frac{\partial f_s^1}{\partial t} + \boldsymbol{v} \cdot \nabla f_s^1 + (\omega_c \tau) \frac{Z_s}{A_s} \left(\boldsymbol{v} \times \boldsymbol{B}^0 \right) \cdot \nabla_{\boldsymbol{v}} f_s^1 + (\omega_c \tau) \frac{Z_s}{A_s} \left(\boldsymbol{E}^1 + \boldsymbol{v} \times \boldsymbol{B}^1 \right) \cdot \nabla_{\boldsymbol{v}} f_s^0 = 0, \quad (4)$$

$$\frac{\partial \mathbf{E}^{1}}{\partial t} - \frac{(\omega_{p}\tau)^{2}}{(\omega_{c}\tau)^{2}} \nabla \times \mathbf{B}^{1} = -\frac{(\omega_{p}\tau)^{2}}{(\omega_{c}\tau)} \mathbf{j}^{1} = -\frac{(\omega_{p}\tau)^{2}}{(\omega_{c}\tau)} \sum_{s} Z_{s} \int \mathbf{v} f_{s}^{1}(\mathbf{x}, \mathbf{v}, t) d\mathbf{v},$$
 (5)

$$\frac{\partial \boldsymbol{B}^1}{\partial t} + \nabla \times \boldsymbol{E}^1 = 0. \tag{6}$$

The azimuthal symmetry established by the equilibrium cyclotron motion about \mathbf{B}^0 leads to a more convenient formulation of the governing equations based on cylindrical velocity-space coordinates $(v_{\perp}, \phi, v_{\parallel})$ with $\mathbf{B}^0 = B^0 \hat{z}$ along the z-axis. This cylindrical velocity space can also be written using Cartesian coordinates through the transformation

$$\boldsymbol{v} = v_{\perp} \cos \phi \hat{\boldsymbol{x}} + v_{\perp} \sin \phi \hat{\boldsymbol{y}} + v_{\parallel} \hat{\boldsymbol{z}}, \tag{7}$$

which is aligned without loss of generality such that waves emanating from the perturbed system can be described by a wave vector given by $\mathbf{k} = k_{\perp} \hat{\mathbf{x}} + k_{\parallel} \hat{\mathbf{z}}$. Following the transformation shown in Ref. [16], the third term in Eq. (4) can be written in terms of the ϕ coordinate, yielding a modified version of this equation given by

$$\frac{\partial f_s^1}{\partial t} + \boldsymbol{v} \cdot \nabla f_s^1 - \omega_{c_s} \left(\omega_c \tau \right) \frac{\partial f_s^1}{\partial \phi} + \left(\omega_c \tau \right) \frac{Z_s}{A_s} \left(\boldsymbol{E}^1 + \boldsymbol{v} \times \boldsymbol{B}^1 \right) \cdot \nabla_{\boldsymbol{v}} f_s^0 = 0, \tag{8}$$

where a species cyclotron frequency is defined as

$$\omega_{c_s} \equiv \frac{Z_s}{A_s} B^0. \tag{9}$$

All perturbed quantities can be expressed in terms of Fourier-transformed plane waves at a particular wave number and frequency, e.g. $f_s^1 = \tilde{f}_s^1 \exp\left[i\left(\mathbf{k}\cdot\mathbf{r} - \omega t\right)\right]$, $\mathbf{E}^1 = \tilde{\mathbf{E}}^1 \exp\left[i\left(\mathbf{k}\cdot\mathbf{r} - \omega t\right)\right]$, where $\mathbf{r} = x\hat{\mathbf{x}} + y\hat{\mathbf{y}} + z\hat{\mathbf{z}}$. Substitution of these forms of the perturbations into Eqs. (8), (5), and (6) leads to

$$(-i\omega + i\boldsymbol{k}\cdot\boldsymbol{v})\,\tilde{f}_s^1 - \omega_{c_s}\,(\omega_c\tau)\,\frac{\partial\tilde{f}_s^1}{\partial\phi} + \frac{Z_s}{A_s}\,(\omega_c\tau)\,\left(\tilde{\boldsymbol{E}}^1 + \boldsymbol{v}\times\tilde{\boldsymbol{B}}^1\right)\cdot\nabla_{\boldsymbol{v}}f_s^0 = 0,\tag{10}$$

$$-i\omega \tilde{\boldsymbol{E}}^{1} = \frac{(\omega_{p}\tau)^{2}}{(\omega_{c}\tau)^{2}} i\boldsymbol{k} \times \tilde{\boldsymbol{B}}^{1} - \frac{(\omega_{p}\tau)^{2}}{(\omega_{c}\tau)} \tilde{\boldsymbol{j}}^{1}, \tag{11}$$

$$-i\omega\tilde{\boldsymbol{B}}^{1} = -i\boldsymbol{k} \times \tilde{\boldsymbol{E}}^{1}. \tag{12}$$

The dispersion relation is obtained by eliminating $\tilde{\boldsymbol{B}}^1$ from Eqs. (10) and (11) using Eq. (12), solving Eq. (10) for \tilde{f}_s^1 , and substituting into Eq. (11) through the current density term, calculated as

$$\tilde{\boldsymbol{j}}^{1} = \sum_{s} Z_{s} \int_{0}^{2\pi} \int_{-\infty}^{\infty} \int_{0}^{\infty} \boldsymbol{v} \tilde{f}_{s}^{1} v_{\perp} dv_{\perp} dv_{\parallel} d\phi \equiv \overline{\overline{\sigma}} \cdot \tilde{\boldsymbol{E}}^{1}.$$
 (13)

This leads to an equation of the form

$$\left(\overline{\overline{I}} + \overline{\overline{\chi}}\right) \cdot \tilde{\boldsymbol{E}}^{1} + \frac{(\omega_{p}\tau)^{2}}{(\omega_{c}\tau)^{2}} \frac{\boldsymbol{k} \times \boldsymbol{k} \times \tilde{\boldsymbol{E}}^{1}}{\omega^{2}} = 0,$$
(14)

where $\overline{\overline{\chi}}$ is the susceptibility tensor and is related to the conductivity tensor $\overline{\overline{\sigma}}$ through the relation

$$\overline{\overline{\chi}} = -\frac{(\omega_p \tau)^2}{i\omega (\omega_c \tau)} \overline{\overline{\sigma}}.$$
 (15)

Evaluation of Eq. (14) requires the solution to Eq. (10). In this work, the problem of interest is described by an equilibrium distribution of the form $f_s^0(v_\perp)$ which is independent of v_\parallel such that $\frac{\partial f_s^0}{\partial v_\parallel} = 0$. In addition, only waves propagating perpendicular to \boldsymbol{B}^0 are considered such that $k_\parallel = 0$. These simplifications, combined with the elimination of $\tilde{\boldsymbol{B}}^1$ through Eq. (12)

as discussed above and some mathematical manipulation leads to a form of Eq. (10) given by

$$\frac{\partial \tilde{f}_s^1}{\partial \phi} - i \left(-\alpha_s + \beta_s \cos \phi \right) \tilde{f}_s^1 = \frac{\omega_{p_s}^2}{Z_s \omega_{c_s}} \frac{\partial F_s^0}{\partial v_\perp} \left[\left(\tilde{E}_x^1 + \frac{k_\perp v_\parallel}{\omega} \tilde{E}_z^1 \right) \cos \phi + \tilde{E}_y^1 \sin \phi \right], \tag{16}$$

where the following variables have been defined:

$$\alpha_s \equiv \frac{\omega}{(\omega_c \tau) \,\omega_{c_s}},\tag{17a}$$

$$\beta_s \equiv \frac{k_{\perp} v_{\perp}}{(\omega_c \tau) \, \omega_{c_s}},\tag{17b}$$

$$F_s^0 \equiv \frac{f_s^0}{n_s},\tag{17c}$$

$$\omega_{p_s}^2 \equiv \frac{Z_s^2 n_s}{A_s}.\tag{17d}$$

After multiplying Eq. (16) with an integrating factor, the expression is then integrated over an unperturbed cyclotron orbit. The resulting integral is evaluated by expanding exponential terms into infinite series of Bessel functions using the identity

$$\exp(-i\beta_s \sin\phi) = \sum_{n=-\infty}^{\infty} \exp(-in\phi) J_n(\beta_s), \qquad (18)$$

where J_n is the Bessel function of the first kind of order n. The expansion simplifies the expression for the perturbed distribution function through the orthogonality property of the Bessel functions.^{16,17} The result of the integration is

$$\tilde{f}_{s}^{1} = i \frac{\omega_{p_{s}}^{2}}{Z_{s}\omega_{c_{s}}} \exp\left(i\beta_{s}\sin\phi\right) \sum_{n=-\infty}^{\infty} \frac{\exp\left(-in\phi\right)}{-\alpha_{s}+n} \frac{\partial F_{s}^{0}}{\partial v_{\perp}} \left[\frac{n}{\beta_{s}} J_{n}\left(\beta_{s}\right) \tilde{E}_{x}^{1} + iJ_{n}'\left(\beta_{s}\right) \tilde{E}_{y}^{1} + \frac{n}{\beta_{s}} \frac{k_{\perp}v_{\parallel}}{\omega} J_{n}\left(\beta_{s}\right) \tilde{E}_{z}^{1}\right].$$
(19)

Equation (19) is then substituted into Eq. (13) and combined with Eq. (15) to yield

$$\overline{\overline{\chi}} = -\frac{2\pi \left(\omega_p \tau\right)^2}{\omega \left(\omega_c \tau\right)} \sum_s \frac{\omega_{p_s}^2}{\omega_{c_s}} \sum_{n=-\infty}^{\infty} \int_0^{\infty} \frac{\partial F_s^0}{\partial v_{\perp}} \begin{pmatrix} \frac{n^2}{\beta_s^2} J_n^2 \left(\beta_s\right) & i \frac{n}{\beta_s} J_n \left(\beta_s\right) J_n' \left(\beta_s\right) \\ -i \frac{n}{\beta_s} J_n \left(\beta_s\right) J_n' \left(\beta_s\right) & J_n' \left(\beta_s\right) J_n' \left(\beta_s\right) \end{pmatrix} \frac{v_{\perp}^2}{-\alpha_s + n} dv_{\perp},$$
(20)

where in this work, all physics of interest is independent of v_{\parallel} , which is thus set to 0. Substitution of Eq. (20) into Eq. (14) yields

$$\begin{pmatrix} K_{11} & K_{12} & 0 \\ K_{21} & K_{22} - \frac{(\omega_p \tau)^2}{(\omega_c \tau)^2} \frac{k_{\perp}^2}{\omega^2} & 0 \\ 0 & 0 & 1 - \frac{(\omega_p \tau)^2}{(\omega_c \tau)^2} \frac{k_{\perp}^2}{\omega^2} \end{pmatrix} \cdot \tilde{\boldsymbol{E}}_1 = 0, \tag{21}$$

where

$$K_{11} = 1 + \overline{\overline{\chi}}_{11},$$
 (22a)

$$K_{12} = \overline{\overline{\chi}}_{12}, \tag{22b}$$

$$K_{21} = \overline{\overline{\chi}}_{21}, \tag{22c}$$

$$K_{22} = 1 + \overline{\overline{\chi}}_{22}.$$
 (22d)

Note the z-component of Eq. (21) decouples and produces a dispersion relation describing the propagation of light waves,

$$\frac{\omega^2}{k_\perp^2} = \frac{(\omega_p \tau)^2}{(\omega_c \tau)^2} = \frac{\frac{q_0^2 n_0}{\epsilon_0 m_0}}{\frac{q_0^2 B_0^2}{m_0^2}} = \frac{n_0 m_0}{\epsilon_0 B_0^2} = \frac{c^2 \mu_0 n_0 m_0}{B_0^2} = \frac{c^2}{v_0^2}.$$
 (23)

If the assumption of $v_{\parallel} = 0$ is not made, the z-component of Eq. (21) would produce an additional term leading to the "ordinary" wave (O-wave), but would still decouple from the rest of the system.¹⁸ Taking the determinant of the remaining 2×2 matrix in Eq. (21) yields another dispersion relation given by

$$D(\omega, k_{\perp}) \equiv K_{11} \left(K_{22} - \frac{(\omega_p \tau)^2}{(\omega_c \tau)^2} \frac{k_{\perp}^2}{\omega^2} \right) - K_{12} K_{21} = 0.$$
 (24)

By inspection, Eq. (24) has poles at $n = \alpha_s$ corresponding to resonances of the cyclotron frequency as well as a double pole at $\omega = 0$. Comparison with the electrostatic dispersion relation presented in Ref. [1] shows that this pole at $\omega = 0$ does not exist in the electrostatic limit.

The solution to Eq. (24) requires the evaluation of Eq. (20), for which the infinite series in $\frac{1}{\overline{\chi}}$ must be truncated to some finite number of terms. However, the series can be removed entirely in favor of Bessel functions of specific orders by employing the Lerche-Newberger sum rule, given by

$$\sum_{n=-\infty}^{\infty} \frac{(-1)^n J_{a-cn}(z) J_{b+cn}(z)}{n+d} = \frac{\pi}{\sin(\pi d)} J_{a+cd}(z) J_{b-cd}(z), \qquad (25)$$

where d is any non-integer complex number, Re(a+b) > -1, and $0 < c \le 1$. Manipulations of the Lerche-Newberger sum rule to remove each infinite series in Eq. (20) are shown

in Ref. [24]. The invocation of the infinite series could also be avoided entirely in solving for \tilde{f}_s^1 in Eq. (16) by taking advantage of the symmetry in particle orbit around the magnetic field during the integration, as shown in Refs. [25,26]. Either approach leads to a form of $\bar{\chi}$ given by

$$\overline{\overline{\chi}} = -\frac{2\pi \left(\omega_p \tau\right)^2}{\omega \left(\omega_c \tau\right)} \sum_s \frac{\omega_{p_s}^2}{\omega_{c_s}} \int_0^\infty \frac{\partial F_s^0}{\partial v_\perp} \begin{pmatrix} \frac{\alpha_s}{\beta_s^2} \left(1 - Q_s\right) & -\frac{i}{2\beta_s} Q_s' \\ \frac{i}{2\beta_s} Q_s' & -\left(\frac{\pi}{\sin(\pi \alpha_s)} J_{-\alpha_s}'\left(\beta_s\right) J_{\alpha_s}'\left(\beta_s\right) + \frac{\alpha_s}{\beta_s^2} \right) \end{pmatrix} v_\perp^2 dv_\perp,$$
(26)

where

$$Q_s \equiv \frac{\pi \alpha_s}{\sin(\pi \alpha_s)} J_{-\alpha_s} (\beta_s) J_{\alpha_s} (\beta_s) , \qquad (27a)$$

$$Q_s' \equiv \frac{\pi \alpha_s}{\sin(\pi \alpha_s)} \frac{\partial}{\partial \beta_s} \left[J_{-\alpha_s} (\beta_s) J_{\alpha_s} (\beta_s) \right]. \tag{27b}$$

Equation (26) is identical to Eq. (20), but has the advantage of removal of the infinite series. Resonances at integer multiples of the cyclotron frequency are also readily apparent through the $\sin(\pi\alpha_s)$ terms in the denominators,²⁵ higher multiples of which would need a large number of terms in the series expansion to accurately resolve $\overline{\chi}$.

The expressions for Q_s , Q'_s , and $J'_{-\alpha_s}J'_{\alpha_s}$ can be recast in a more convenient form in terms of integrals of real low-order Bessel functions, given by

$$J_{-\alpha_s}(\beta_s) J_{\alpha_s}(\beta_s) = \frac{2}{\pi} \int_0^{\frac{\pi}{2}} J_0(2\beta_s \cos \theta) \cos(2\alpha_s \theta) d\theta, \qquad (28a)$$

$$\frac{\partial}{\partial \beta_s} \left[J_{-\alpha_s} \left(\beta_s \right) J_{\alpha_s} \left(\beta_s \right) \right] = -\frac{4}{\pi} \int_0^{\frac{\pi}{2}} J_1 \left(2\beta_s \cos \theta \right) \cos \theta \cos \left(2\alpha_s \theta \right) d\theta, \tag{28b}$$

$$J_{-\alpha_s}'(\beta_s)J_{\alpha_s}'(\beta_s) = \frac{1}{\pi} \left[\int_0^{\frac{\pi}{2}} \cos(2\alpha_s \theta) \left[J_2(2\beta_s \cos \theta) - J_0(2\beta_s \cos \theta) \cos(2\theta) \right] d\theta - \frac{\alpha_s}{\beta_s^2} \sin(\pi \alpha_s) \right].$$

$$(28c)$$

Details of this derivation can be found in Appendix A.

By specifying the equilibrium distribution functions, specifically $\frac{\partial f_0^s}{\partial v_{\perp}}$, the system of equations given by Eqs. (22), (24), and (26) provides a closed-form implicit expression for the

electromagnetic dispersion relation for the DGH instability. The integrals in Eq. (28), which are needed by Eq. (26), can be evaluated to arbitrary accuracy using numerical quadrature.

While the derivation in this section is restricted to $k_{\parallel} = 0$ waves and to distributions of the form $f_s^0(v_{\perp})$, the procedure can be extended to evaluate the full susceptibility tensor, written for infinite sums of real integer order Bessel functions as shown in Ref. [16] or products of complex order Bessel functions as shown in Ref. [25], where these restrictions are not made. The integrals in Eq. (28) are sufficient to calculate the full susceptibility tensor shown in Ref. [25] where $k_{\parallel}v_{\parallel}$ is incorporated into Eq. (17a) and where a parallel velocity dependence is added to the equilibrium distribution function such that $f_s^0 = f_s^0(v_{\perp}, v_{\parallel})$. The numerical integration of the resulting equation similar to Eq. (26) would have the added complication of poles resulting from v_{\parallel} in denominators when there is finite k_{\parallel} , which can be handled using analytic continuation techniques as shown by Landau²⁷ and Bernstein⁴ for unmagnetized and magnetized waves, respectively.

The generalization of the wave vector from $\mathbf{k} = k_{\perp}\hat{\mathbf{x}}$ and the distribution function velocity dependence from $f_s^0(v_{\perp})$ also provides a natural development path to benchmark kinetic codes in higher dimensions beyond 1D2V. The extension to two spatial dimensions can be realized by generalizing k_{\perp} to the x-y plane such that $\mathbf{k} = k_{\perp,x}\hat{\mathbf{x}} + k_{\perp,y}\hat{\mathbf{y}}$, which allows for benchmarking of 2D2V codes. Allowing for parallel velocity dependence of the equilibrium distribution function, such that $f_s^0 = f_s^0(v_{\perp}, v_{\parallel}) = f_s^0(v_x, v_y, v_z)$, and adding a parallel component to the wave vector such that it lies in the x-z plane where $\mathbf{k} = k_{\perp}\hat{\mathbf{x}} + k_{\parallel}\hat{\mathbf{z}}$ leads to a 3×3 susceptibility tensor that can be calculated as described above and can be used to benchmark 2D3V codes simulating oblique wave propagation. Further generalization of the wave vector such that $\mathbf{k} = k_{\perp,x}\hat{\mathbf{x}} + k_{\perp,y}\hat{\mathbf{y}} + k_{\parallel}\hat{\mathbf{z}}$ analogous to the extension from 1D2V to 2D2V can also allow for benchmarking of 3D3V codes.

IV. CALCULATION OF THE DISPERSION RELATION FOR SPECIFIC FORMS OF $f_s^0(v_\perp)$, VALUES OF k_\perp , AND ω_p/ω_c RATIO

The electromagnetic dispersion relation derived in Sec. III can be used to determine the linear behavior of an equilibrium ring distribution in conditions leading to the DGH

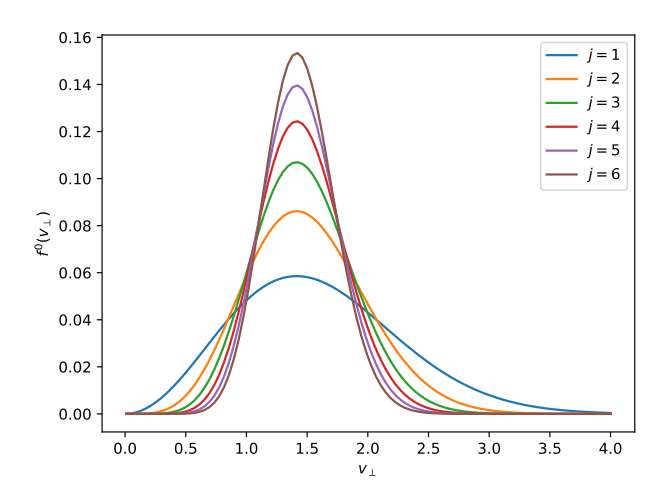


FIG. 1. Equilibrium ring distribution function for the DGH instability for various j. The distribution is peaked at $v_{\perp 0} = j^{1/2}\alpha_{\perp}$. The thickness of the distribution can be measured by its half-width at half-maximum, approximated by $\alpha_{\perp}/2$, which scales with $j^{-1/2}$ for a given $v_{\perp 0}$. Distribution functions with j = 1, 2, 6 correspond to cases A-D where $v_{\perp 0} = \sqrt{2}$ as described in Table I.

instability. The specific form of the ring distribution studied by Dory et al.⁷ is given by

$$f^{0}(v_{\perp}) = \frac{1}{\pi \alpha_{\perp}^{2} j!} \left(\frac{v_{\perp}^{2}}{\alpha_{\perp}^{2}}\right)^{j} \exp\left(-\frac{v_{\perp}^{2}}{\alpha_{\perp}^{2}}\right), \tag{29}$$

which has a derivative which can be calculated analytically, yielding

$$\frac{\partial f^0}{\partial v_{\perp}} = \frac{1}{\pi \alpha_{\perp}^2 j!} \frac{2v_{\perp}}{\alpha_{\perp}^2} \exp\left(-\frac{v_{\perp}^2}{\alpha_{\perp}^2}\right) \left(\frac{v_{\perp}^2}{\alpha_{\perp}^2}\right)^{j-1} \left[j - \left(\frac{v_{\perp}^2}{\alpha_{\perp}^2}\right)\right]. \tag{30}$$

The peak velocity of the distribution is given by $v_{\perp 0} = j^{1/2}\alpha_{\perp}$ while the half-width at half-maximum (HWHM) is approximated by $\alpha_{\perp}/2^{28}$ which is incorrectly presented in Ref. [1] and in Ref. [7]. This relationship between j and distribution width for a fixed $v_{\perp 0}$ can be seen in Fig. 1. The distribution is found to be unstable if sufficiently peaked, the ratio of plasma frequency to cyclotron frequency is above a certain value known as the density threshold, and the wave number falls within a specified range.^{1,7}

To illustrate the electromagnetic extension of the DGH instability, four specific cases are examined of a ring distribution of electrons in the presence of a static neutralizing background of ions ($A_{\rm e}=1,\ Z_{\rm e}=-1,\ f_{\rm e}^0=f^0,\ f_{\rm i}^1=0$). The parameters of this distribution for these cases are shown in Table I where $\tilde{k}\equiv k_{\perp}v_{\perp0}\frac{\omega_p}{\omega_c}$ is a normalized wave number. For all cases $v_{\perp0}=\sqrt{2}$ and $B^0=1$. Cases A-C are identical to cases examined in Ref. [1],

Case	j	ω_p/ω_c	$ ilde{k}$	α_{\perp}	HWHM	β
A	6	20	3.15	$\sqrt{1/3}$	$\sqrt{1/3}/2$	1/6
В	6	20	4.65	$\sqrt{1/3}$	$\sqrt{1/3}/2$	1/6
С	2	10	2.12	1	1/2	1/2
D	1	1	2.12	$\sqrt{2}$	$\sqrt{2}/2$	1

TABLE I. Parameters for distribution f^0 for the various cases under consideration, each with $v_{\perp 0} = \sqrt{2}$ and $B^0 = 1$. Cases A-C correspond to cases in Ref. [1] while Case D is introduced with lower j and ω_p/ω_c , which is stable according to both the electromagnetic and electrostatic dispersion relations.

where case A was found to have a purely growing instability, case B was found to be unstable with an oscillatory behavior, and case C was found to be stable according to the electrostatic dispersion relation. These same cases are re-examined using the more general electromagnetic theory. Case D is introduced with decreased j, widening the distribution which reduces peakedness, and a lower plasma to cyclotron frequency ratio which further moves the plasma below the density threshold for instability. The DGH mode is completely stabilized when j = 0, corresponding to Maxwellian distribution functions.^{1,7} Table I also calculates plasma beta of the electrons, given by

$$\beta = \frac{2nT}{(B^0)^2} = \frac{n\alpha_{\perp}^2 A}{2(B^0)^2},\tag{31}$$

where T is calculated from the thermal velocity which is approximated by the half-width at half-maximum of the distribution given by $v_{\rm th} = \sqrt{T/A} = \alpha_{\perp}/2$, and where n = 1 and A = 1 for electrons. The electrostatic approximation is valid for $\beta \ll 1$, which inspection of Eq. (31) shows becomes less accurate for hotter distributions.

The electromagnetic dispersion relation for each case is examined and compared with the electrostatic dispersion relation derived in Ref. [1]. The characteristic time is set to $\tau \equiv \omega_p^{-1}$, leading to $\omega_p \tau = 1$ and $\omega_c \tau = (\omega_p/\omega_c)^{-1}$. Integrations required in the electromagnetic dispersion relation as derived in Sec. III as well as those required in the electrostatic dispersion relation as derived in Ref. [1] are performed using the second-order accurate trapezoidal rule³⁰ using 100 points. The electromagnetic and electrostatic dispersion relations for cases A, B, C, and D are plotted in Figs. 2, 3, 4, and 5, respectively, where the frequencies are normalized to the cyclotron frequency ($\tilde{\omega} = \omega_{\frac{\omega_p}{\omega_c}}$). Shown also are zero contours of the real

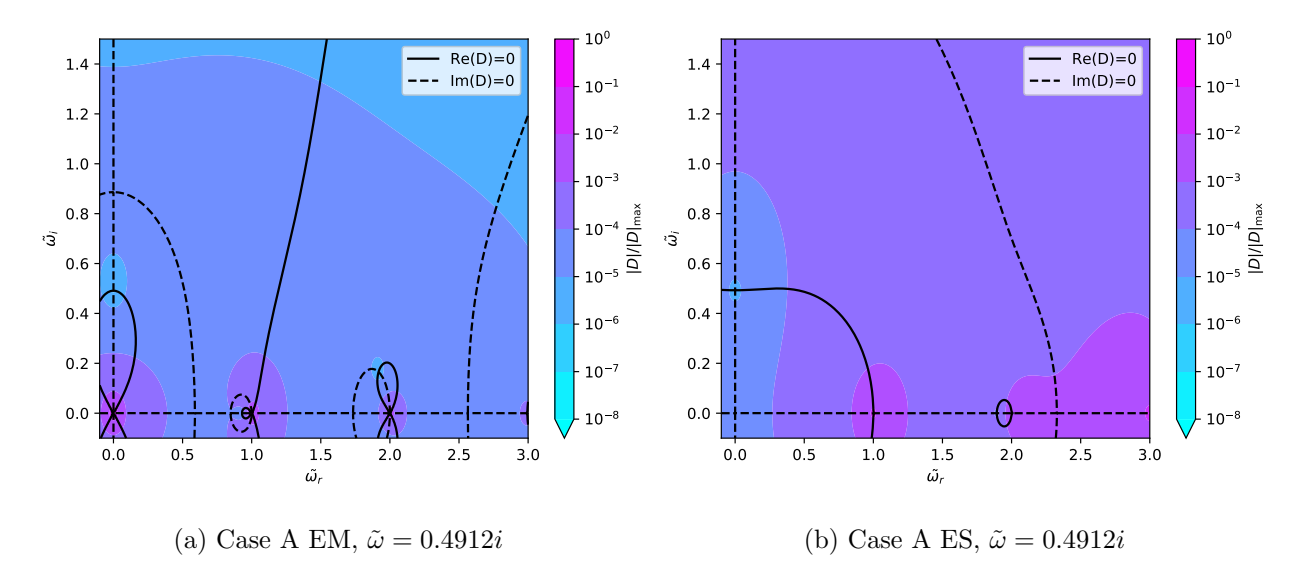


FIG. 2. Filled contours for normalized magnitudes of the electromagnetic (EM) and electrostatic (ES) dispersion relations for case A plotted on a 320×320 grid with $\tilde{\omega}_r \in [-0.1, 3.0]$ and $\tilde{\omega}_i \in [-0.1, 1.5]$ with line contours of Re(D) = 0 and Im(D) = 0 overlaid. These contour lines cross at roots of $D(\omega, k_{\perp}) = 0$ as well as poles of $D(\omega, k_{\perp})$. Solutions to the dispersion relation exist at the roots but not at the poles. The poles exist at real integer multiples of the cyclotron frequency for both the EM and ES dispersion relations, with an extra pole at 0 for the EM dispersion relation. For this case, the largest growing mode written as $\tilde{\omega}$ underneath each contour plot, given by the root of $D(\omega, k_{\perp}) = 0$ with the largest imaginary component, agrees well for the EM and ES dispersion relations and is purely imaginary.

and imaginary components of the dispersion relation. Solutions exist where the real and imaginary zero contours intersect, satisfying $D(\omega, k_{\perp}) = 0$, but not at the poles of $D(\omega, k_{\perp})$ indicated by $|D|/|D|_{\text{max}}$ approaching unity. After the general vicinity of a solution is found, more precise calculations are performed with a Newton–Raphson method, using more points in the trapezoidal rule of integration until convergence to $\tilde{\omega}$ within 10^{-4} is reached.

The complex frequencies from the electrostatic and electromagnetic dispersion relations are found to be close for cases A and B. However for case C, the results and behavior characteristics deviate. The electromagnetic dispersion relation shows growth and oscillation while the electrostatic dispersion relation produces multiple purely real frequencies. This discrepancy can by understood by the high plasma beta of the distribution, as seen in Table I, indicating the inaccuracy of the electrostatic theory. Case D yields purely real

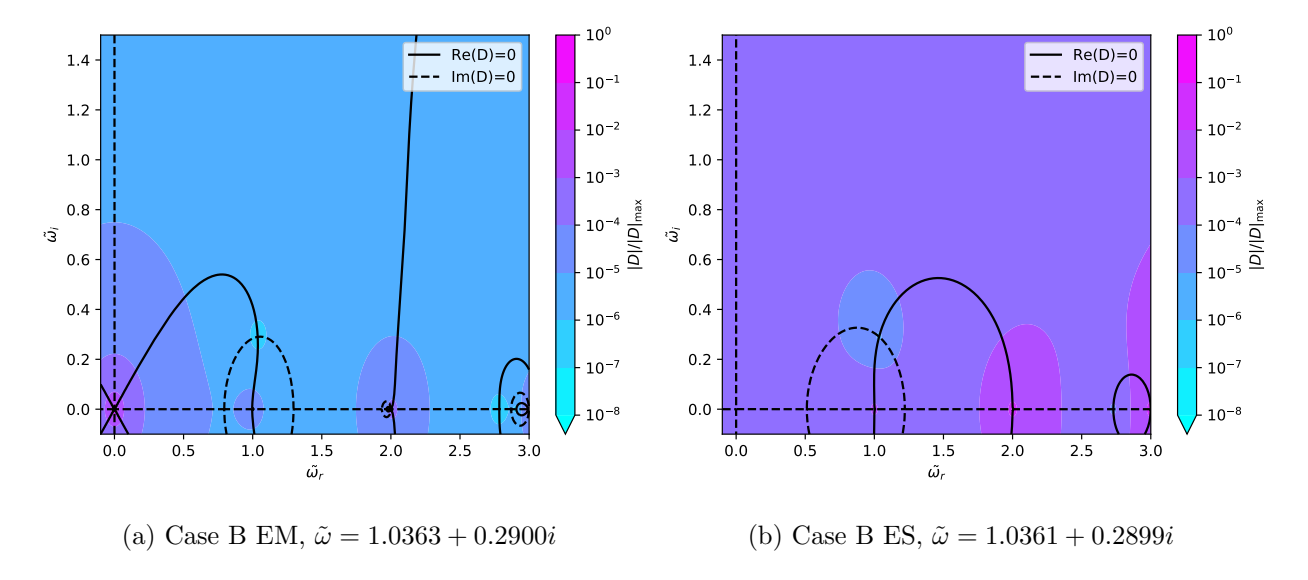


FIG. 3. Filled contours for normalized magnitudes of the EM and ES dispersion relations for case B with line contours of Re(D) = 0 and Im(D) = 0 overlaid as in Fig. 2. For this case, the root of $D(\omega, k_{\perp}) = 0$ corresponding to the largest growing mode agrees well for the ES and EM dispersion relations and has mixed oscillatory and imaginary components.

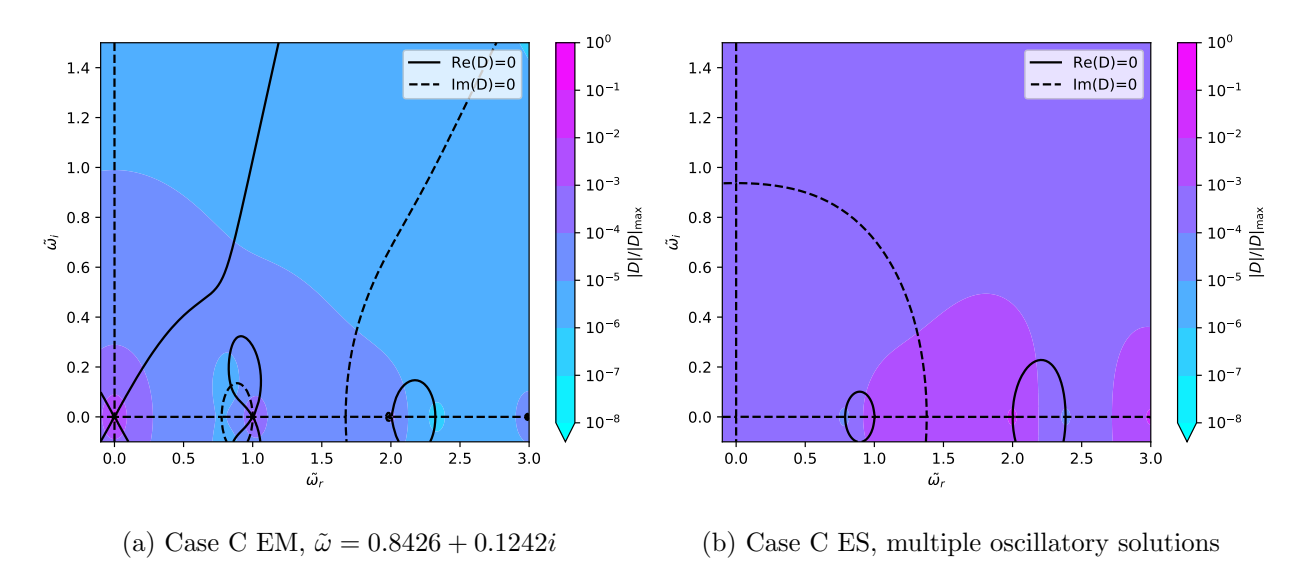
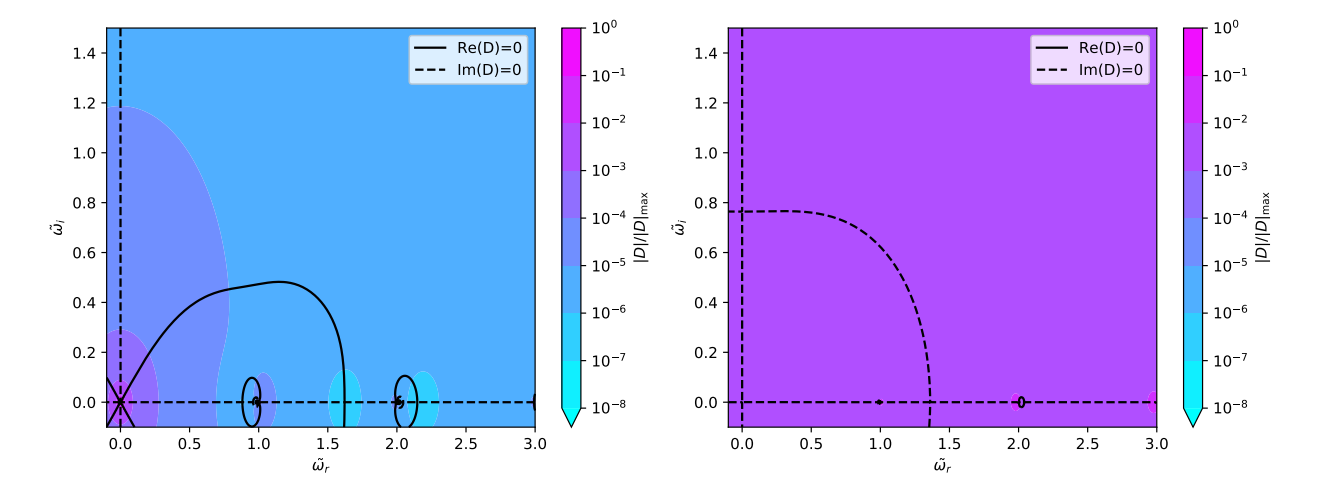


FIG. 4. Filled contours for normalized magnitudes of the EM and ES dispersion relations for case C with line contours of Re(D) = 0 and Im(D) = 0 overlaid as in Fig. 2. For this case, the root of $D(\omega, k_{\perp}) = 0$ for the EM dispersion relation corresponding to the largest growing mode has mixed oscillatory and imaginary components while the ES dispersion relation has no growing solutions.



- (a) Case D EM, multiple oscillatory solutions
- (b) Case D ES, multiple oscillatory solutions

FIG. 5. Filled contours for normalized magnitudes of the EM and ES dispersion relations for case D with line contours of Re(D) = 0 and Im(D) = 0 overlaid as in Fig. 2. For this case, no growing roots of $D(\omega, k_{\perp}) = 0$ exist for either the EM or ES dispersion relations.

frequencies for both the electrostatic and electromagnetic dispersion relations. The absence of growth can be explained by the further widening of the distribution and decreased plasma to cyclotron frequency ratio compared to the other cases. Even with the increased plasma beta of this distribution indicating inaccuracy of the electrostatic theory, the combination of increased temperature and reduced frequency ratio makes this case stable even using the electromagnetic dispersion relation, which is not true in case C.

The next sections verify these observations using continuum kinetic simulations of the Vlasov-Maxwell system.

V. NUMERICAL METHOD FOR THE VLASOV-MAXWELL SYSTEM

The Vlasov equation as described in Eq. (1) is rewritten in conservative form,

$$\frac{\partial f_s}{\partial t} + \nabla \cdot (\boldsymbol{v} f_s) + \nabla_{\boldsymbol{v}} \cdot \left[(\omega_c \tau) \frac{Z_s}{A_s} (\boldsymbol{E} + \boldsymbol{v} \times \boldsymbol{B}) f_s \right] = 0.$$
 (32)

Maxwell's equations, Eqs. (2) and (3), can also be written in conservative form, such that the entire governing equation system can be expressed compactly as

$$\frac{\partial \boldsymbol{q}}{\partial t} + \nabla \cdot \boldsymbol{\mathcal{F}} = \boldsymbol{\mathcal{S}},\tag{33}$$

where q is the solution vector for the equation set, \mathcal{F} is the flux tensor, and \mathcal{S} represents source terms. The x coordinate is generalized to position x and velocity v for the Vlasov equation, Eq. (32).

Expressing the governing equation system in the form of Eq. (33) facilitates solution with the discontinuous Galerkin finite element method using the WARPXM (Washington Approximate Riemann Plasma) framework.³¹ The framework provides algorithms that solve plasma physics problems on unstructured grids using fluid models as well as the continuum kinetic model described by the Vlasov-Maxwell equation system. The code subdivides a simulation domain into discrete elements and projects conservation variables onto a set of basis functions ϕ_m of order m such that the numerical approximation is represented as

$$q = \sum_{m} q_{m} \phi_{m}. \tag{34}$$

Equation (33) is then multiplied by each basis function and integrated over each element volume Ω , yielding the weak form integral equation for each basis function given by

$$\int_{\Omega} \frac{\partial \mathbf{q}}{\partial t} \phi_m dV + \oint_{\partial \Omega} \mathbf{F} \cdot \mathbf{n} \phi_m dS - \int_{\Omega} \mathbf{F} \cdot \nabla \phi_m dV = \int_{\Omega} \mathbf{S} \phi_m dV, \tag{35}$$

where the divergence theorem has been applied to the flux tensor term. Equation (35) is solved using an explicit Runge-Kutta (ERK) time-stepping method. This combination of spatial and temporal discretizations produces a compact, high-order scheme with an optimal convergence rate of $\mathcal{O}(h^{N+1})$ for element size h and polynomial basis order $N.^{32}$ Lagrange interpolating polynomials based on Legendre-Gauss-Lobatto quadrature node locations are used for the basis functions, yielding a nodal scheme in which the coefficients in Eq. (34) correspond to solution values at the node locations. Further details of the discontinuous Galerkin method used in the WARPXM framework can be found in Refs. [33,34]. A discussion on the appropriate fluxes in the surface integral for the Vlasov and Maxwell equations as well as of the ERK time-stepping algorithm used to evolve Eq. (35) can be found in Ref. [15]. For the ERK schemes, the allowable timestep is determined by the CFL condition

$$\Delta t \le C \left(\sum_{d=1}^{D} \frac{a_d}{h_d} \right)^{-1}, \tag{36}$$

where C is the Courant number, D=3 is the number of phase-space dimensions, a_d is the maximum advection speed in direction d, and h_d is a measure of the element spacing in direction d. Courant numbers are set based on those defined for various combinations of ERK scheme and basis order.³⁵

VI. NUMERICAL SIMULATIONS OF THE DGH INSTABILITY AND COMPARISON TO THEORY

The four cases described in Sec. IV are simulated using the discontinuous Galerkin algorithm described in Sec. V. For each simulation, the electric field energy, given by

$$U_{\rm E} = \frac{1}{2} \int E^2 dx \tag{37}$$

is calculated and plotted on a semi-log scale from which the growth rate, $\tilde{\omega}_i$ and oscillation frequency, $\tilde{\omega}_r$ can be measured. The ring distribution given in Eq. (29) is initialized on a Cartesian grid of $x \in [0, \frac{2\pi}{k_{\perp}}]$ and $v_x, v_y \in [-4, 4]$ with a perturbation such that the initial electron distribution is given by

$$f(x, v_x, v_y)|_{t=0} = \frac{1}{\pi \alpha_{\perp}^2 j!} \left(\frac{v_x^2 + v_y^2}{\alpha_{\perp}^2} \right)^j \exp\left(-\frac{v_x^2 + v_y^2}{\alpha_{\perp}^2} \right) \left[1 + \epsilon \sin\left(4 \arctan\left(\frac{v_y}{v_x} \right) - k_{\perp} x \right) \right],$$
(38)

where $\epsilon = 10^{-4}$. Reference [1] uses the same perturbed distribution and demonstrated effective excitation of the dominant mode. Simulations are performed on a phase-space grid of resolutions given by $N_x \times N_{v_x} \times N_{v_y}$: $48 \times 24 \times 24$, $56 \times 28 \times 28$, $64 \times 32 \times 32$, and $80 \times 40 \times 40$. Second-order polynomial basis elements characterized by third-order optimal spatial convergence³² are used with fourth-order ERK time-stepping. The Courant number used in all simulations is 0.235 in accordance with Ref. [35].

Figure 6a shows a plot of the electric field energy measured at every t=5 for the $80 \times 40 \times 40$ resolution simulation for all cases, where the growth rates given by $\tilde{\omega}_i$ are measured using the slopes of line fits through the data. The growth rates for cases A-C are in line with the theoretical values predicted by the electromagnetic dispersion relation, while a small growth is seen for case D despite no prediction of growth from the theory. This small growth seen for case D may be a nonlinear effect due to the coupling of real frequency solutions to the dispersion relation excited from the perturbation profile in Eq. (38). Fast Fourier transforms (FFTs) are calculated for each case after the linear growth has been subtracted to determine the oscillation frequencies given by $\tilde{\omega}_r$, which are shown in Fig. 6b. Mixed growth and oscillation is expected for cases B and C according to the electromagnetic dispersion relation as shown in Sec. IV. The oscillation frequencies are found to be at the peaks of the FFT spectra. For case B, the oscillation frequency is calculated as the average

Case	$\tilde{\omega}_i^{\mathrm{th,EM}}$	$\tilde{\omega}_i^{\mathrm{th,ES}}$	$\tilde{\omega}_i^{\mathrm{num}}$	$\varepsilon_i^{\mathrm{EM}}$	$\tilde{\omega}_r^{ ext{th,EM}}$	$\tilde{\omega}_r^{ ext{th,ES}}$	$ ilde{\omega}_r^{ ext{num}}$	$\varepsilon_r^{\mathrm{EM}}$
A	0.4912	0.4912	0.4956	0.9%	-	-	-	-
В	0.2900	0.2899	0.2965	2.2%	1.0363	1.0361	1.0357 ± 0.0690	<6.7%
C	0.1242	_	0.1239	0.2%	0.8426	-	0.8240 ± 0.0515	<6.1%
D	-	-	0.0018	-	-	-	-	1

TABLE II. Theoretical growth rates and oscillation frequencies of the electromagnetic and electrostatic dispersion relations as calculated in Sec. IV as well as numerical results from discontinuous Galerkin simulations of the Vlasov-Maxwell system. Growth rates are converged values as shown in Fig. 7, and oscillation frequencies for cases B and C are calculated from FFTs of the $80 \times 40 \times 40$ simulation. The errors between numerical results and electromagnetic theory are calculated as $\varepsilon_{i,r}^{\rm EM} = \left| \tilde{\omega}_{i,r}^{\rm num} - \tilde{\omega}_{i,r}^{\rm th,EM} \right| / \tilde{\omega}_{i,r}^{\rm th,EM}$.

of the first peak, found to be at $\tilde{\omega}_r^B=1.0357\pm0.0690$ while for case C, the peak is found at $\tilde{\omega}_r^C=0.8240\pm0.0515$, where in both cases half the frequency bin size is specified as the uncertainty. These frequencies are found to be independent of resolution. The growth rates however can be compared for various resolutions to obtain converged values. Figure 7 shows the convergence from the simulations performed at the four resolutions described by plotting growth versus velocity-space resolution and line fitting to find the limit as element size approaches zero. The converged results are summarized in Table II along with theoretical values for the electromagnetic and electrostatic dispersion relations calculated in Sec. IV. Theoretical oscillation frequencies and those measured from the simulation results with the FFTs are also given in Table II. The growth rate convergence is calculated assuming a rate of order 3 for second-order basis functions used in simulations. The growth rate discrepancies for cases A and C are less than 1% while the discrepancy for case B is 2.2%. The error in oscillation frequency as measured by the FFT should be less than 6.7% for case B and less than 6.1% for case C, based on the frequency resolution.

The simulation results show agreement with the theoretical predictions from the electromagnetic dispersion relations. They also confirm the agreement between the electrostatic approximation and the electromagnetic model for the cases of lower plasma beta in A and B. The agreement between electromagnetic theory and simulation in case C shows that with increased plasma beta, the electrostatic approximation is inadequate to accurately predict

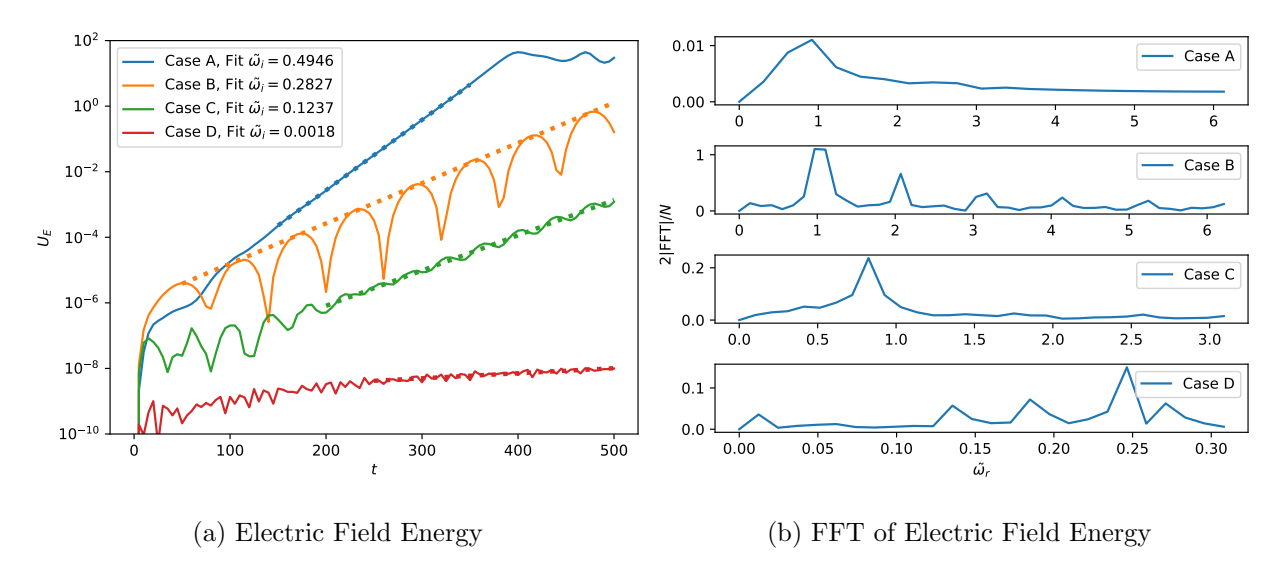


FIG. 6. Simulations of the DGH instability with the Vlasov-Maxwell system using $80 \times 40 \times 40$ second-order polynomial elements. Figure 6a shows the growth of the electric field energy for cases A-D, where t is normalized by ω_p . Line fits showing the slope yielding $\tilde{\omega}_i$ are also shown for the times during which the linear growth is measured. The measurement durations are $t \in [150, 350]$, [50, 500], [200, 500], and [250, 500] for cases A, B, C, and D, respectively. For case B, the line fit is based on the peaks of the oscillation. Figure 6b shows absolute values of the fast Fourier transforms for each case for these times, after the linear growth has been subtracted to remove the zero-frequency component and the result at negative frequencies are combined with those at positive frequencies. The peaks in the FFT plots correspond to the oscillation frequency, $\tilde{\omega}_r$. For case B, the oscillation frequency is calculated as the average of the first peak, yielding $\tilde{\omega}_r^B = 1.0357 \pm 0.0690$. For case C, the oscillation frequency is found at the first peak to be $\tilde{\omega}_r^C = 0.8240 \pm 0.0515$.

instabilities involving perpendicular waves. In case D, both theories predict stability and a small growth is seen in simulation.

VII. CONCLUSIONS

A closed-form integral representation of the electromagnetic dispersion relation for the DGH instability is derived using electromagnetic theory, which is more complete than the electrostatic approximation that is only valid for low-beta plasmas. Theoretical growth rates and oscillation frequencies are computed for four cases of equilibrium electron ring distribu-

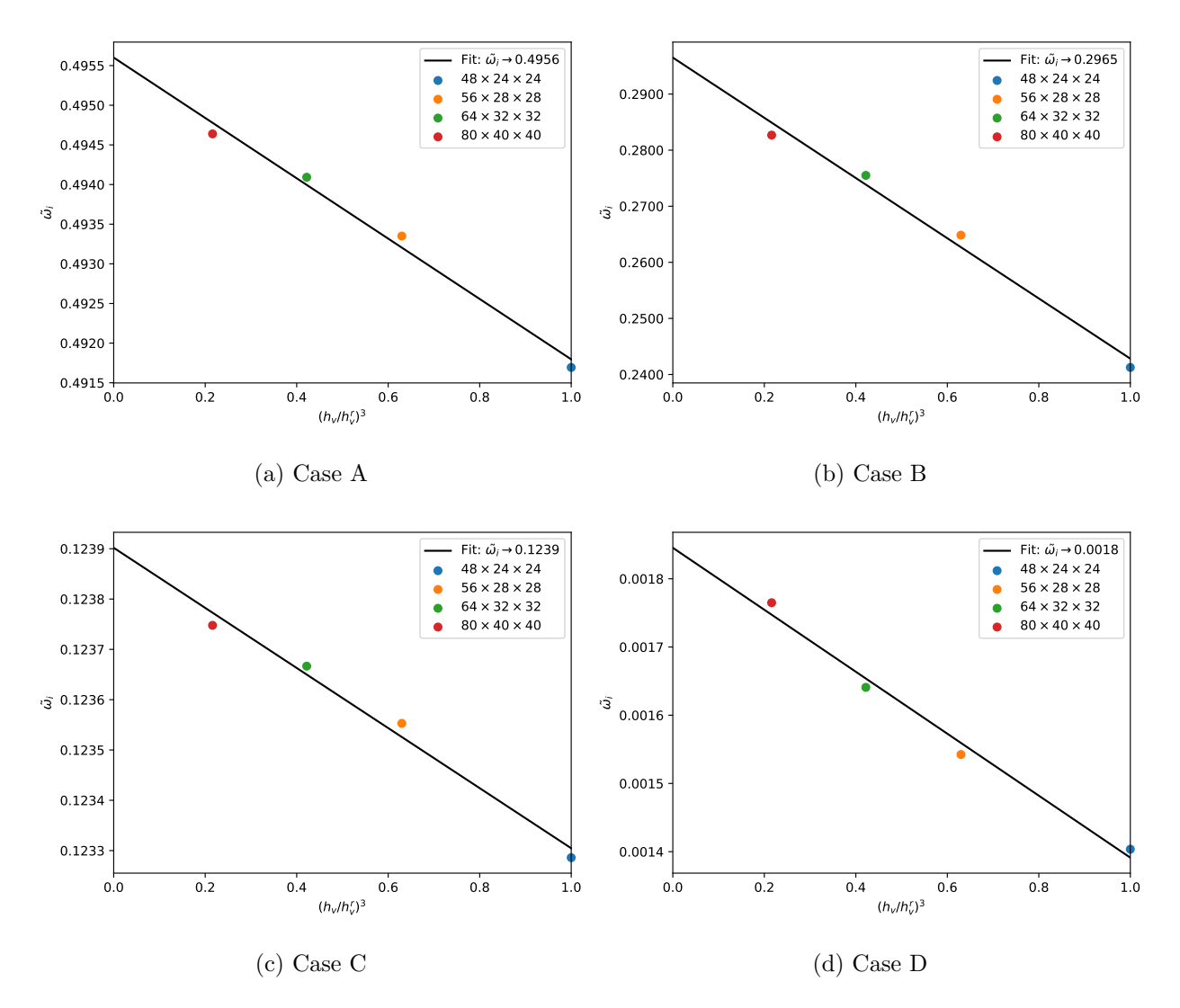


FIG. 7. Convergence of growth rates $\tilde{\omega}_i$ for cases A-D. The growth rates are plotted for various resolutions against a velocity-space element length (h_v) normalized to the reference element length of a $48 \times 24 \times 24$ velocity-space element (h_v) with the expected cubic spatial convergence. Line fits are constructed to determine the y-intercepts corresponding to the $\lim_{h_v \to 0} \tilde{\omega}_i$.

tions using electromagnetic and electrostatic dispersion relations. As predicted, agreement between the electromagnetic and electrostatic dispersion relations is found in the growth rates and oscillation frequencies for cases characterized by low plasma beta. A case with increased temperature (and corresponding increased plasma beta) and reduced plasma to cyclotron frequency ratio to further move the plasma below the density threshold for instability was predicted by the electrostatic dispersion relation to be stable but unstable according to electromagnetic theory. Simulations using WARPXM to solve the continuum

kinetic Vlasov-Maxwell system in 1D2V confirm the electromagnetic dispersion results. A case with further increased temperature reducing the peakedness of the distribution and reduced plasma to cyclotron frequency ratio is found to be stable according to both theories, even though less confidence can be given to the electrostatic dispersion relation due to the corresponding increased plasma beta. The Vlasov-Maxwell simulations for this case show a small growth, possibly due to nonlinear effects.

The agreement between simulation results and theory confirm the use of the DGH instability as a viable benchmark for continuum kinetic codes solving the Vlasov-Maxwell system for plasmas subject to dynamic magnetic fields and currents. The electromagnetic generalization extends the analysis of the DGH instability using the electrostatic approximation confined to plasmas characterized by small beta such as those of cold ring distributions to include higher beta plasmas with higher temperatures. In addition, the closed-form integral representation of the electromagnetic dispersion relation derived in this work can be used as a benchmark for other numerical treatments of the Vlasov-Maxwell system, such as electromagnetic particle-in-cell methods.

ACKNOWLEDGMENTS

The authors would like to thank A. Ho and G. V. Vogman for stimulating discussions. The information, data, or work presented herein was funded in part by the Air Force Office of Scientific Research under award numbers FA9550-15-1-0271. This material is also based upon work supported by the National Science Foundation under Grant No. PHY-2108419.

DATA AVAILABILITY STATEMENT

The data that support the findings of this study are available from the corresponding author upon reasonable request.

Appendix A: Recasting products of Bessel functions of complex order in terms of integrals of Bessel functions of real order

The electromagnetic susceptibility in Eq. (26) of the DGH instability resulted in an expression containing products of complex order Bessel functions which are difficult to treat

numerically. However, by applying Neumann's formula^{36,37}

$$J_{\nu}(z) J_{\mu}(z) = \frac{2}{\pi} \int_{0}^{\frac{\pi}{2}} J_{\nu+\mu}(2z\cos\theta)\cos\left[\left(\mu-\nu\right)\theta\right] d\theta \tag{A1}$$

$$\operatorname{Re}(\nu+\mu) > -1,$$

these products can be recast in terms of integrals of real order Bessel functions. Application of Eq. (A1) on the product $J_{-\alpha_s}(\beta_s) J_{\alpha_s}(\beta_s)$ leads to

$$J_{-\alpha_s}(\beta_s) J_{\alpha_s}(\beta_s) = \frac{2}{\pi} \int_{0}^{\frac{\pi}{2}} J_0(2\beta_s \cos \theta) \cos(2\alpha_s \theta) d\theta.$$
 (A2)

Differentiation of Eq. (A2) yields

$$\frac{\partial}{\partial \beta_{s}} \left[J_{-\alpha_{s}} \left(\beta_{s} \right) J_{\alpha_{s}} \left(\beta_{s} \right) \right] = \frac{2}{\pi} \frac{\partial}{\partial \beta_{s}} \int_{0}^{\frac{\pi}{2}} J_{0} \left(2\beta_{s} \cos \theta \right) \cos \left(2\alpha_{s} \theta \right) d\theta$$

$$= \frac{2}{\pi} \int_{0}^{\frac{\pi}{2}} \frac{\partial J_{0} \left(2\beta_{s} \cos \theta \right)}{\partial \left(2\beta_{s} \cos \theta \right)} \frac{\partial \left(2\beta_{s} \cos \theta \right)}{\partial \beta_{s}} \cos \left(2\alpha_{s} \theta \right) d\theta$$

$$= \frac{2}{\pi} \int_{0}^{\frac{\pi}{2}} \frac{\partial J_{0} \left(2\beta_{s} \cos \theta \right)}{\partial \left(2\beta_{s} \cos \theta \right)} 2 \cos \theta \cos \left(2\alpha_{s} \theta \right) d\theta. \tag{A3}$$

Application of the recurrence relation

$$J_{\nu-1}(z) - J_{\nu+1}(z) = 2\frac{\partial}{\partial z} [J_{\nu}(z)],$$
 (A4)

and identity for integer n^{37}

$$J_{-n}(z) = (-1)^n J_n(z), \tag{A5}$$

on the derivative term yields

$$\frac{\partial J_0 \left(2\beta_s \cos \theta\right)}{\partial \left(2\beta_s \cos \theta\right)} = \frac{1}{2} \left[J_{-1} \left(2\beta_s \cos \theta\right) - J_1 \left(2\beta_s \cos \theta\right) \right]
= \frac{1}{2} \left[-J_1 \left(2\beta_s \cos \theta\right) - J_1 \left(2\beta_s \cos \theta\right) \right]
= -J_1 \left(2\beta_s \cos \theta\right).$$
(A6)

Substitution of Eq. (A6) into Eq. (A3) results in

$$\frac{\partial}{\partial \beta_s} \left[J_{-\alpha_s} \left(\beta_s \right) J_{\alpha_s} \left(\beta_s \right) \right] = -\frac{4}{\pi} \int_0^{\frac{\pi}{2}} J_1 \left(2\beta_s \cos \theta \right) \cos \theta \cos \left(2\alpha_s \theta \right) d\theta. \tag{A7}$$

 $J'_{-\alpha_s}(\beta_s) J'_{\alpha_s}(\beta_s)$ can also be simplified, first by substitution of Eq. (A4), yielding

$$J'_{-\alpha_{s}}(\beta_{s}) J'_{\alpha_{s}}(\beta_{s}) = \frac{1}{2} \left[J_{-\alpha_{s}-1}(\beta_{s}) - J_{-\alpha_{s}+1}(\beta_{s}) \right] \frac{1}{2} \left[J_{\alpha_{s}-1}(\beta_{s}) - J_{\alpha_{s}+1}(\beta_{s}) \right]$$

$$= \frac{1}{4} \left[\underbrace{J_{-\alpha_{s}-1}(\beta_{s}) J_{\alpha_{s}-1}(\beta_{s})}_{A} - \underbrace{J_{-\alpha_{s}-1}(\beta_{s}) J_{\alpha_{s}+1}(\beta_{s})}_{B} - \underbrace{J_{-\alpha_{s}+1}(\beta_{s}) J_{\alpha_{s}-1}(\beta_{s})}_{B} + \underbrace{J_{-\alpha_{s}+1}(\beta_{s}) J_{\alpha_{s}+1}(\beta_{s})}_{D} \right], \tag{A8}$$

where the terms A-D have been defined for convenience and will be treated separately using Eq. (A1). However for the term $A = J_{-\alpha_s-1}(\beta_s) J_{\alpha_s-1}(\beta_s)$, Eq. (A1) cannot be used directly because Re $(\nu + \mu) = -2 < -1$. This term can be rewritten using the recurrence relation for complex ν^{37}

$$J_{\nu+1}(z) + J_{\nu-1}(z) = \frac{2\nu}{z} J_{\nu}(z),$$
 (A9)

yielding

$$A = J_{-\alpha_{s}-1}(\beta_{s}) J_{\alpha_{s}-1}(\beta_{s}) = \left[\frac{-2\alpha_{s}}{\beta_{s}} J_{-\alpha_{s}}(\beta_{s}) - J_{-\alpha_{s}+1}(\beta_{s})\right] \left[\frac{2\alpha_{s}}{\beta_{s}} J_{\alpha_{s}}(\beta_{s}) - J_{\alpha_{s}+1}(\beta_{s})\right]$$

$$= \frac{-4\alpha_{s}^{2}}{\beta_{s}^{2}} \underbrace{J_{-\alpha_{s}}(\beta_{s}) J_{\alpha_{s}}(\beta_{s})}_{E} + \underbrace{\frac{2\alpha_{s}}{\beta_{s}}}_{F} \underbrace{J_{-\alpha_{s}+1}(\beta_{s}) J_{\alpha_{s}+1}(\beta_{s})}_{F}$$

$$- \underbrace{\frac{2\alpha_{s}}{\beta_{s}}}_{G} \underbrace{J_{-\alpha_{s}+1}(\beta_{s}) J_{\alpha_{s}}(\beta_{s})}_{G} + \underbrace{J_{-\alpha_{s}+1}(\beta_{s}) J_{\alpha_{s}+1}(\beta_{s})}_{D}, \tag{A10}$$

where terms E-G have also been defined for convenience. Term E is given by Eq. (A2). Application of Eq. (A1) on the remaining terms yields

$$B = J_{-\alpha_s - 1}(\beta_s) J_{\alpha_s + 1}(\beta_s) = \frac{2}{\pi} \int_0^{\frac{\pi}{2}} J_0(2\beta_s \cos \theta) \cos \left[(2\alpha_s + 2) \theta \right] d\theta, \tag{A11}$$

$$C = J_{-\alpha_s+1}(\beta_s) J_{\alpha_s-1}(\beta_s) = \frac{2}{\pi} \int_0^{\frac{\pi}{2}} J_0(2\beta_s \cos \theta) \cos \left[(2\alpha_s - 2) \theta \right] d\theta, \tag{A12}$$

$$D = J_{-\alpha_s+1}(\beta_s) J_{\alpha_s+1}(\beta_s) = \frac{2}{\pi} \int_{0}^{\frac{\pi}{2}} J_2(2\beta_s \cos \theta) \cos(2\alpha_s \theta) d\theta,$$
 (A13)

$$F = J_{-\alpha_s}(\beta_s) J_{\alpha_s+1}(\beta_s) = \frac{2}{\pi} \int_0^{\frac{\pi}{2}} J_1(2\beta_s \cos \theta) \cos \left[(2\alpha_s + 1) \theta \right] d\theta, \tag{A14}$$

$$G = J_{-\alpha_s+1}(\beta_s) J_{\alpha_s}(\beta_s) = \frac{2}{\pi} \int_0^{\frac{\pi}{2}} J_1(2\beta_s \cos \theta) \cos \left[(2\alpha_s - 1) \theta \right] d\theta. \tag{A15}$$

Substitution of Eqs. (A2) and (A10)-(A15) into Eq. (A8) produces

$$J'_{-\alpha_{s}}(\beta_{s}) J'_{\alpha_{s}}(\beta_{s}) = \frac{1}{4} (A - B - C + D)$$

$$= \frac{1}{4} \left[\frac{-4\alpha_{s}^{2}}{\beta_{s}^{2}} E + \frac{2\alpha_{s}}{\beta_{s}} F - \frac{2\alpha_{s}}{\beta_{s}} G + D - B - C + D \right]$$

$$= \frac{1}{4} \left[\frac{-4\alpha_{s}^{2}}{\beta_{s}^{2}} E - B - C + \frac{2\alpha_{s}}{\beta_{s}} (F - G) + 2D \right]$$

$$= \frac{1}{2\pi} \left[-\int_{0}^{\frac{\pi}{2}} J_{0} (2\beta_{s} \cos \theta) \left[\frac{4\alpha_{s}^{2}}{\beta_{s}^{2}} \cos (2\alpha_{s}\theta) + \cos \left[(2\alpha_{s} + 2)\theta \right] + \cos \left[(2\alpha_{s} - 2)\theta \right] \right] d\theta$$

$$+ \frac{2\alpha_{s}}{\beta_{s}} \int_{0}^{\frac{\pi}{2}} J_{1} (2\beta_{s} \cos \theta) \left\{ \cos \left[(2\alpha_{s} + 1)\theta \right] - \cos \left[(2\alpha_{s} - 1)\theta \right] \right\} d\theta$$

$$+ 2 \int_{0}^{\frac{\pi}{2}} J_{2} (2\beta_{s} \cos \theta) \cos (2\alpha_{s}\theta) d\theta \right]. \tag{A16}$$

The integrals involving J_0 and J_1 can be further simplified by using the cosine sum trigonometric identity

$$\cos(a+b) = \cos a \cos b - \sin a \sin b, \tag{A17}$$

yielding

$$J'_{-\alpha_s}(\beta_s) J'_{\alpha_s}(\beta_s) = \frac{1}{\pi} \left[-\int_0^{\frac{\pi}{2}} J_0(2\beta_s \cos \theta) \cos(2\alpha_s \theta) \left[\frac{2\alpha_s^2}{\beta_s^2} + \cos(2\theta) \right] d\theta - \frac{2\alpha_s}{\beta_s} \int_0^{\frac{\pi}{2}} J_1(2\beta_s \cos \theta) \sin \theta \sin(2\alpha_s \theta) d\theta + \int_0^{\frac{\pi}{2}} J_2(2\beta_s \cos \theta) \cos(2\alpha_s \theta) d\theta \right].$$
(A18)

The integral involving J_1 can be removed by relating it to an integral involving J_0 by integrating Eq. (A2) by parts and employing Eq. (A6), yielding

$$\int_{0}^{\frac{\pi}{2}} J_1(2\beta_s \cos \theta) \sin \theta \sin (2\alpha_s \theta) d\theta = \frac{\sin (\pi \alpha_s)}{2\beta_s} - \frac{\alpha_s}{\beta_s} \int_{0}^{\frac{\pi}{2}} J_0(2\beta_s \cos \theta) \cos (2\alpha_s \theta) d\theta.$$
 (A19)

Substitution of Eq. (A19) into Eq. (A18) yields

$$J_{-\alpha_s}'(\beta_s)J_{\alpha_s}'(\beta_s) = \frac{1}{\pi} \left[\int_0^{\frac{\pi}{2}} \cos(2\alpha_s \theta) \left[J_2(2\beta_s \cos \theta) - J_0(2\beta_s \cos \theta) \cos(2\theta) \right] d\theta - \frac{\alpha_s}{\beta_s^2} \sin(\pi \alpha_s) \right]. \tag{A20}$$

Equations (A2), (A7), and (A20) recast the products of complex-order Bessel functions in the susceptibility tensor in Eq. (26) as integrals of real integer-order Bessel functions which can be evaluated using standard scientific computing packages. This allows for numerical evaluation of the electromagnetic dispersion relation for the DGH instability given in Eq. (24).

REFERENCES

- ¹G. V. Vogman, P. Colella, and U. Shumlak, Journal of Computational Physics **277**, 101 (2014).
- ²J. Juno, A. Hakim, J. TenBarge, E. Shi, and W. Dorland, Journal of Computational Physics **353**, 110 (2018).
- ³J. W. Banks and J. A. F. Hittinger, IEEE Transactions on Plasma Science **38**, 2198 (2010).

- ⁴I. B. Bernstein, Physical Review **109**, 10 (1958).
- ⁵J. A. Tataronis and F. W. Crawford, Journal of Plasma Physics 4, 231 (1970).
- ⁶A. V. Timofeev and V. I. Pistunovich, in *Reviews of Plasma Physics*, edited by M. A. Leontovich (Springer, Boston, MA, 1970) Chap. 3, pp. 401–445.
- ⁷R. A. Dory, G. E. Guest, and E. G. Harris, Physical Review Letters **14**, 131 (1965).
- $^8\mathrm{R.~F.}$ Post and M. N. Rosenbluth, Physics of Fluids 9, 730 (1966).
- ⁹R. F. Hubbard and T. J. Birmingham, Journal of Geophysical Research 83, 4837 (1978).
- ¹⁰S. Perraut, A. Roux, P. Robert, R. Gendrin, J. Sauvaud, J. Bosqued, G. Kremser, and A. Korth, Journal of Geophysical Research 87, 6219 (1982).
- ¹¹S. V. Singh, A. P. Kakad, R. V. Reddy, and G. S. Lakhina, Journal of Plasma Physics **70**, 613 (2004).
- ¹²E. Ott, B. Hui, and K. R. Chu, The Physics of Fluids **23**, 1031 (1980).
- ¹³G. Taylor, Fusion Science and Technology **52**, 119 (2007).
- ¹⁴F. W. Crawford, Nuclear Fusion **5**, 73 (1965).
- 15 A. Ho, I. A. M. Datta, and U. Shumlak, Frontiers in Physics $\bf 6$, 105 (2018).
- ¹⁶D. A. Gurnett and A. Bhattacharjee, Introduction to Plasma Physics With Space, Laboratory and Astrophysical Applications (Cambridge University Press, New York, New York, 2017).
- ¹⁷T. H. Stix, Waves In Plasmas (API, New York, New York, 1992) pp. 250–256.
- $^{18}\mathrm{W}.$ E. Drummond and M. N. Rosenbluth, The Physics of Fluids 2, 45 (1960).
- ¹⁹I. Lerche, The Physics of Fluids **9**, 1073 (1966).
- ²⁰I. Lerche, Plasma Physics **16**, 955 (1974).
- $^{21}\mathrm{B.~S.}$ Newberger, Journal of Mathematical Physics $\mathbf{23},\,1278$ (1982).
- $^{22}\mathrm{B.~S.}$ Newberger, Journal of Mathematical Physics $\mathbf{24},\,2250$ (1983).
- ²³I. Lerche, R. Schlickeiser, and R. C. Tautz, Physics of Plasmas **15**, 024701 (2008).
- ²⁴G. D. Swanson, *Plasma Waves*, 2nd ed. (Institute of Physics Publishing, Bristol, UK, 2003).
- ²⁵H. Qin, C. K. Phillips, and R. C. Davidson, Physics of Plasmas **14**, 092103 (2007).
- $^{26}\mathrm{H.}$ Qin, C. K. Phillips, and R. C. Davidson, Physics of Plasmas $\mathbf{15},\,024702$ (2008).
- ²⁷L. Landau, Journal of Physics **10**, 25 (1946).
- ²⁸The peak velocity of f^0 is determined by finding the positive root of $f^{0'} = \frac{\partial f^0}{\partial v_{\perp}} = 0$, yielding $v_{\perp 0} \equiv v_{\perp}(f^{0'} = 0) = j^{1/2}\alpha_{\perp}$. An approximation of the distribution width, which

- is used for the estimation of the half-width at half-maximum and thermal velocity, is determined by finding the inflection points on either side of the peak, calculated from roots of $f^{0''}(v_{\perp}) = \frac{\partial^2 f^0}{\partial v_{\perp}^2} = 0$, where the term $\sqrt{16j+1}$ is simplified by assuming 16j >> 1, yielding $v_{\perp}(f^{0''} = 0) \approx v_{\perp 0} \pm \alpha_{\perp}/2$.
- ²⁹A. B. Mikhailovskii, *Electromagnetic Instabilities in an Inhomogenous Plasma*, Vol. 1 (IOP Publishing Ltd, New York, New York, 1992) p. xvii.
- ³⁰J. Stoer and R. Bulirsch, *Introduction to Numerical Analysis*, 3rd ed. (Springer Science+Business Media, LLC, New York, NY, 2002).
- ³¹U. Shumlak, R. Lilly, N. Reddell, E. Sousa, and B. Srinivasan, Computer Physics Communications **182**, 1767 (2011).
- ³²J. S. Hesthaven and T. Warburton, Nodal Discontinuous Galerkin Methods: Algorithms, Analysis, and Applications (Springer Science+Business Media, LLC, New York, USA, 2008).
- ³³J. Loverich and U. Shumlak, Computer Physics Communications **169**, 251 (2005).
- ³⁴J. Loverich, A. Hakim, and U. Shumlak, Communications in Computational Physics 9, 240 (2011).
- ³⁵B. Cockburn and C.-W. Shu, Journal of Scientific Computing **16**, 173 (2001).
- ³⁶B. G. Korenev, *Bessel Functions and their Applications* (Taylor & Francis, London, UK, 2002).
- ³⁷A. Erdélyi, W. Magnus, F. Oberhettinger, F. Tricomi, and H. Bateman, Higher Transcendental Functions, California Institute of Technology H. Bateman Manuscript Project, Vol. 2 (McGraw-Hill, New York, NY, 2003).